sustainability

MDPI

Article

The Optimal Dispatch of a Power System Containing Virtual Power Plants under Fog and Haze Weather

Yajing Gao *, Huaxin Cheng, Jing Zhu, Haifeng Liang and Peng Li

Received: 25 November 2015; Accepted: 8 January 2016; Published: 13 January 2016
Academic Editor: Tatiana Morosuk

School of Electrical and Electronic Engineering, North China Electric Power University, Baoding 071003, China; hxxxdsxb@163.com (H.C.); ncepuzhujing@163.com (J.Z.); hfliang@ncepu.edu.cn (H.L.); ncepulp@gmail.com (P.L.)
* Correspondence: commoncat@163.com; Tel.: +86-137-2228-2201

Abstract: With the growing influence of fog and haze (F-H) weather and the rapid development of distributed energy resources (DERs) and smart grids, the concept of the virtual power plant (VPP) employed in this study would help to solve the dispatch problem caused by multiple DERs connected to the power grid. The effects of F-H weather on photovoltaic output forecast, load forecast and power system dispatch are discussed according to real case data. The wavelet neural network (WNN) model was employed to predict photovoltaic output and load, considering F-H weather, based on the idea of "similar days of F-H". The multi-objective optimal dispatch model of a power system adopted in this paper contains several VPPs and conventional power plants, under F-H weather, and the mixed integer linear programming (MILP) and the Yalmip toolbox of MATLAB were adopted to solve the dispatch model. The analysis of the results from a case study proves the validity and feasibility of the model and the algorithms.

Keywords: fog and haze; virtual power plant; forecast; wavelet neural network; optimal dispatch; mixed integer linear programming

1. Introduction

Challenges in the energy industry, such as rapidly growing demands for electricity, low efficiency of energy utilization and deteriorating environmental conditions, have attracted increasing global attention. Currently, thermal power plants (TPPs) of multiple sizes located all over the country are the major generators of power in China's electricity market. TPPs are characterized by a high consumption of coal resources, which is one of the main factors of air pollution. The air pollution, which contains harmful gases, solid particles in the air and the greenhouse effect resulting from excessive emissions of CO_2, has affected people's livelihood and caused many problems in the operation, maintenance and dispatch control of power systems.

The air quality in China continues to deteriorate, and fog and haze weather (F-H) has become a new weather condition that is attracting much attention by the government and the public because its influence area has gradually increased. In 2013, more than 100 cities in 25 provinces in China, which represent 25% of the national territorial area, were covered by F-H [1]. The severity level of F-H can be quantitatively described by the Air Quality Index (AQI), which is a dimensionless index calculated by the contents of SO_2, CO_2, PM10 (inhalable particle matter, diameter <10 μm), PM2.5 (fine particulate matter, diameter <2.5 μm), CO and O_3 [2]. The AQI level (L_{AQI}) ranges from Level 1–Level 6 (0–50, 51–100, 101–150, 151–200, 201–300 and >300), which correspond to excellent condition, good condition, slight pollution, moderate pollution, severe pollution and serious pollution. People should consciously avoid outdoor activities when L_{AQI} is above Level 4, especially children, the elderly and patients with heart, respiratory and lung diseases.

The Chinese government has attempted several measures in the long run to restrict the impacts of F-H: introducing a variety of energy-saving equipment and employing new energy-saving technology to reduce the consumption of fossil fuels, substituting electricity for coal in industrial manufacturing to effectively control pollutant emissions and transforming the emissions technology of TPPs and other industries to realize solidified treatment of air pollutants. In addition, several emergency measures are taken when the F-H condition is serious. For instance, to ensure the smooth operation of the military parade in Beijing that commemorated the 70th anniversary of the victory in the Anti-Japanese War, the government took several temporary control measures with regard to public traffic, industries and construction sites to reduce the emission of air pollutants. The above measures were highly effective and brought the "blue sky of military parade" to Beijing temporarily. The mean concentration of PM2.5 in Beijing was 17.8 $\mu g/m^3$, and the air quality was excellent ($L_{AQI} = 1$) from 20 August–3 September 2015. However, Beijing was covered by F-H again after the anniversary. During the period of Chinese National Day holidays, the Air Quality Index (AQI) values in Beijing from 1–3 October 2015 were all lower than 60, whereas the air condition deteriorated from 4–7 October 2015, and the largest AQI value reached 335. Therefore, a long-term method is urgently needed to overcome F-H weather.

The environmental benefits of a strategy of sustainable development have been emphasized, and clean energy that is abundant and renewable will gradually replace conventional fossil energy. Therefore, the permeability of distributed energy resources (DERs), which consist of distributed generation (intermittent power generation, controllable power generation, *etc.*), electrical energy storage (static energy storage, electric vehicles, *etc.*) and demand response resources (controllable load, efficiency resources, *etc.*), would increase. The demerits of DERs, such as multiple and changeable output characteristics, various scales, decentralization, uncertainties, difficulties of distribution networks to absorb DERs, lower automation levels, outdated control strategies of dispatch and lack of interaction and communication between the power grid and consumers [3], greatly restrict the popularity of DERs. More control power is needed if a large number of DERs are connected to the grid directly, which would cause some complexity in the system control. A micro-grid that aggregates scattered DERs to form a single controllable unit could centrally control various DERs and weaken the impact on system stability [4,5]. However the micro-grid is strict in its configuration and cannot be disassembled and reassembled at will. The objective of the micro-grid in early studies focused on the local application of DERs, which had some limitations on the large-scale application of scattered DERs.

The concept of the virtual power plant (VPP) is employed in this paper to solve the above problems [6–11]. There is no universally-accepted definition for VPPs, and recent theoretical studies and applications have mainly been reported in the European and American regions, such as flexible electricity network to integrate expected energy solution project (FENIX) and electric vehicles in distributed and integrated market using sustainable energy and open networks (EDISON). The VPP, which comprises controllable energy units (generations, consumers and prosumers) and can be controlled (centralized or decentralized) in order to alter the electricity production (like any other conventional units), is not a real power plant. In this paper, the VPP is defined as a special virtual unit that logically aggregates diverse DERs distributed in the generation and consumption sides, based on information and communication technology, increasing the visibility and enhancing the controllability of DERs in the power grid. The external performance of the VPP is the overall characteristic of DERs, and the VPP center internally controls the operation of all DERs.

The operation control of the VPP mainly concentrates on two points: On the one hand, previous studies have researched the strategies that power systems integrally control VPPs at the grid level to make plans for power generating and purchasing according to optimal power flow and maximum economic benefits of VPPs or other conventional power plants, the objectives of which contain the profit of electricity sale, power purchase cost, ancillary service profit of the spinning reserve, generation cost of DERs, charge-discharge cost of electrical energy storage, compensatory payment for demand response resources, *etc.* [6–8]. For instance, research on VPPs that contain electric vehicles (EVs) have focused on operating plans considering generating and start-up (shut-down) costs of distributed

generations (DGs), fees of battery aging and system power balance constraints [9,10]. On the other hand, the methods by which the VPP internally controls the aggregated DERs, based on a mathematical programming model and a multi-agent system, have been researched, as well [6,11]. The internal control of the VPP has three different structures: centralized structure (all of the information of the power generation and consumption is available to the VPP center), centralized-decentralized structure (there are several subordinate control units of the VPP center) and decentralized structure (the information transformation relies on the multi-agent system). In conclusion, previous studies emphatically researched measures for capacity allocation, coordinated operation, operation control and market bidding participation to maximize the benefits of VPPs or power systems from the perspective of VPPs. In this paper, the VPP dispatch strategies at the grid level that consider the impacts of F-H weather are discussed.

F-H weather would still exist in vast areas of China, and strategies of the operation, maintenance, prediction and dispatch control of power systems under F-H weather need improving. As for the predictions, the early studies about photovoltaic output and load forecasts only consider traditional meteorological factors, such as temperature, humidness and all kinds of weather types, rarely focusing on F-H [12,13]. The literature [14] has proven that illumination intensity is directly blocked by F-H, and the instantaneous output and effective operating time of photovoltaic panels (PV panels) are greatly restricted. Residents' modes of production and life are affected by F-H, as well. People would stay indoors for health reasons, and industries with high energy consumption and high emission would be shut down by the government's contingency plan to reduce pollutant emission when the air is seriously polluted [15]. Therefore, a suitable prediction model that considers the F-H factor is urgently needed, which would increase the reliability of photovoltaic output and load forecasts. Besides, the power system control center should distribute more power load to the generation with low emission during dispatch periods when L_{AQI} is high, yet this has been addressed by few studies.

In this paper, the impacts of F-H on photovoltaic output and power load are first analyzed, and the wavelet neural network (WNN) model is adopted to predict photovoltaic output and load under F-H, based on the idea of similar days of F-H. On that basis, the power system multi-objective optimal dispatch model containing VPPs under F-H is employed to achieve the goals of energy conservation and emission reduction. The main contents in this paper comprise the following six parts: F-H impacts on photovoltaic output and load forecasts (Section 2); the dispatch of power systems containing VPPs (Section 3); the mathematical model of dispatch under F-H weather (Section 4); solving the optimal dispatch model based on mixed integer linear programming (MILP) (Section 5); case study (Section 6); conclusions (Section 7).

2. F-H Impacts on Photovoltaic Output and Load Forecasts

On 7 December 2015, the Moderate Resolution Imaging Spectroradiometer on NASA's Aqua satellite captured an image of eastern China being inundated by thick F-H, seen in the gray area of Figure 1.

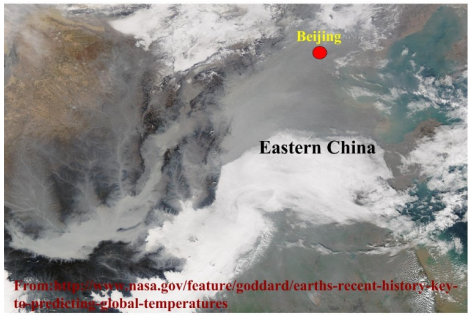

Figure 1. The spatial distribution of fog and haze of eastern China on 7 December 2015.

As shown in Figure 1, the thick F-H would certainly block out sunlight, which would affect the output of PV panels to a great extent. The previous day in Beijing, the Chinese government issued a first-ever "red alert" for the city, which resulted in power plant and factory closures and the change of power load.

The generation output forecast (photovoltaic power, wind power, thermal power, *etc.*) and load forecast of power systems are the basic tasks of dispatching, in which improved prediction accuracy would efficiently reduce the complexity and uncertainty of dispatch control to ensure the system's safe, economic and green operation. The impacts of F-H on photovoltaic output and power load are discussed as follows.

2.1. The Influence of F-H on Photovoltaic Output

The discontinuity, instability and uncertainty issues surrounding photovoltaic output are directly affected by meteorological factors, in which different weather conditions lead to different incident light intensity on PV panels. The incident light on PV panels is weakened only by atmosphere and clouds when no F-H is present. Otherwise, some light intensity is reflected and absorbed by F-H. Light intensity and photovoltaic output are further weakened with a high AQI level. Moreover, more dust appears on PV panels with increasing AQI level, which greatly restricts photoelectric conversion efficiency, as well. Thus, timely dust cleaning is needed.

The AQI values of Baoding, China, from 24–26 February 2015 are shown in Table 1, and the photovoltaic outputs of the polycrystalline silicon photovoltaic array (PSPA, 10 kW) in the State Key Laboratory of New Energy Power System (SKL of NEPS) at the North China Electric Power University (NCEPU, Baoding) during the same period are shown in Figure 2.

Table 1. Air quality of Baoding, China, from 24–26 February 2015. AQI, Air Quality Index.

Date	AQI	AQI Level	PM2.5	PM10	CO	NO_2	SO_2
24 February 2015	337	Serious/6	265	442	4.13	58	111
25 February 2015	180	Moderate/4	136	247	2.2	36	68
26 February 2015	98	Good/2	68	108	1.89	38	92

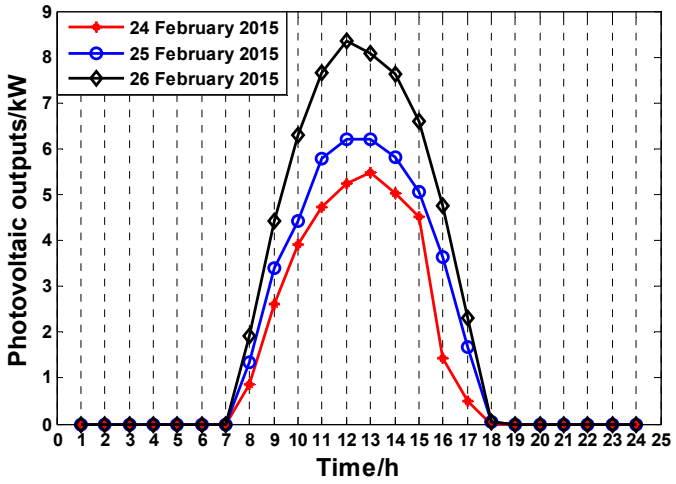

Figure 2. Photovoltaic outputs of the polycrystalline silicon photovoltaic array (PSPA) (10 kW) in the State Key Laboratory of New Energy Power System (SKL of NEPS) at the North China Electric Power University (NCEPU) from 24–26 February 2015.

As shown in Table 1 and Figure 2, the daily photovoltaic outputs (kW) of 24 February, 25 February and 26 February are 34.31 (L_{AQI} = 2), 43.64 (L_{AQI} = 4) and 58.06 (L_{AQI} = 6), which indicates that photovoltaic output decreases with increasing AQI level.

In addition, the number of effective power generating hours (NEPGH) of PV panels may decrease with increasing F-H, which could also reduce photovoltaic output. Data from an empirical research platform of a photovoltaic system at the Chinese Academy of Sciences (Shanghai) indicated that the NEPGH was 2.79 on 4 December 2013 when F-H did not exist. However, the NEPGH was reduced to only 0.7, which was a reduction of 74.91%, on 6 December 2013, when the air condition included severe pollution. Therefore, the impact of F-H should be considered during the prediction process of photovoltaic output.

2.2. The Influence of F-H on Load

Several emergency warning policies are implemented by the Chinese government when F-H is serious, and the emergency warning levels, from low to high, are indicated by the colors yellow, orange and red according to forecast data of severity and continuous days of F-H. The influence of F-H on load could be divided into two parts:

(1) Load directly influenced by emergency warning policies:

The Chinese government forcibly shuts down some industries under conditions of heavy pollution and high energy consumption (or calls for reducing production) to reduce pollutant emission when emergency warning policies are implemented. The reduced portion of the load is directly influenced by the emergency warning policies. For instance, the daily load of a cement plant in Baoding, China, from 20–29 December 2014 is shown in Figure 3.

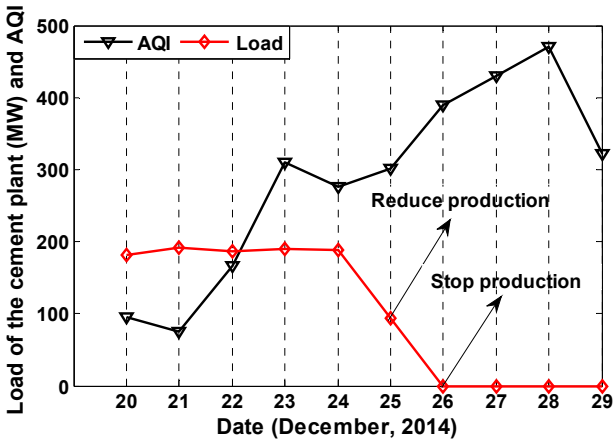

Figure 3. Daily load of a cement plant in Baoding, China, from 20–29 December 2014.

As shown in Figure 3, although the air condition indicated serious pollution on 23 December, there was no emergency warning signal on 22 December, because the AQI value would drop in the foreseeable future. Thus, the cement plant did not reduce production or shut down. The AQI value would stay at a high level and continue to rise after 24 December. Therefore, the emergency warning signal became red on 24 December. As a result, production of the cement plant was reduced by nearly 50% on 25 December, and it was shut down forcibly from 26–29 December.

(2) Load not directly influenced by emergency warning policies:

The other portions of the load are not directly influenced by emergency warning policies, such as residential load and commercial load. These portions of load with higher randomness, which vary with people's subjective consciousness, are also affected by F-H. Considering the residential load as an example, the daily load of a residential quarter in Baoding, China, from 20–29 December 2014 is shown in Figure 4.

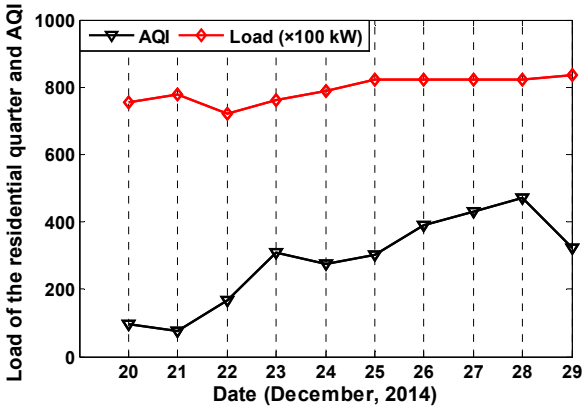

Figure 4. Daily load of a residential quarter in Baoding, China, from 20–29 December 2014.

The Pearson's correlation coefficient, which is shown in Formula (1), is employed to analyze the correlation between curves of the AQI and load in Figure 4.

$$r = \frac{\sum_{i=1}^{n}(x_i - \overline{x})(y_i - \overline{y})}{\sqrt{\sum_{i=1}^{n}(x_i - \overline{x})^2}\sqrt{\sum_{i=1}^{n}(y_i - \overline{y})^2}} \quad (1)$$

where x_i and y_i (i = 1,2, . . . ,n) are the values of the AQI and the load.

According to the raw data of Figure 4, the correlation coefficient r = 0.7164, which indicates that the AQI and daily residential load have a relatively strong positive correlation. Residents consciously stay home under F-H weather to keep healthy; therefore, residential load would increase to some degree.

In all, industrial load is the main controllable load directly affected by emergency warning policies under F-H weather. The total power consumption of the whole Chinese society in the first quarter of 2014 was 1.28 × 10^{14} kW, a year-to-year growth of 5.4%, the growth rate of which increased by 1.1%. However, the growth rate dropped by 3% from the last quarter of 2013, because some industries with heavy pollution and high energy consumption were forced to reduce production or shut down by the government of North China to control F-H weather.

For example, the AQI values of Baoding, China, from 17–28 November 2013 and the daily total load (including industrial load, residential load, commercial load, *etc.*) of a region in Baoding, China, during the same period are shown in Figure 5.

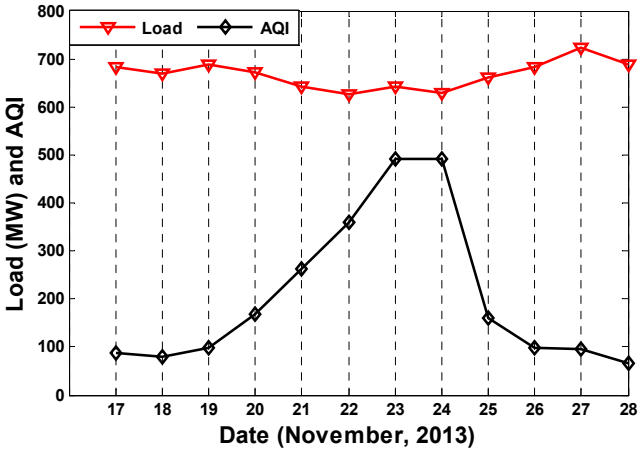

Figure 5. Daily total load of a region in Baoding, China, from 17–28 November 2013.

According to the raw data of Figure 5, the correlation coefficient $r = -0.8230$, which indicates that the AQI and daily total load have a relatively strong negative correlation, and the accuracy would be improved to some degree if the AQI factor is considered in the load forecast.

2.3. Selection of "Similar Days of F-H"

The prediction accuracy of photovoltaic output and load forecasts would improve to some degree if input data were selected from days with a similar temperature, light intensity, weather type, day type, *etc.* The above analysis indicates that there are great similarities in photovoltaic outputs (or loads) under the same AQI level, which cannot be ignored. Therefore, the idea of similar days of F-H is introduced in this paper, which emphasizes F-H weather based on the former research.

(1) Select similar days of F-H for photovoltaic output:

Step 1. Data preprocessing:

The order of magnitudes of different data varies greatly, which makes it difficult for any model to implement predictions. Therefore, data should be normalized or mapped to the range of [0,1] before calculating according to Formula (2):

$$Y = \frac{X - X_{\min}}{X_{\max} - X_{\min}} \tag{2}$$

where X is one of the samples; $X_{\max}$ and $X_{\min}$ are the maximal and minimal values of samples; Y is the normalized value of X.

Besides, the relation of weather types and their values could be listed as follows: sunny, 1.0; cloudy, 0.9; overcast, 0.8; rainy, 0.6; snowy, 0.2; sunny to cloudy, 0.95; cloudy to overcast, 0.85; overcast to rainy, 0.75; cloudy to snowy, 0.45; *etc.* [15].

Step 2. Principal component analysis (PCA):

Traditional methods to select similar days need more calculation time on account of the enormous raw data volume. The PCA is a statistical method that could convert multiple variables X_i (i = 1,2, ... ,n) into a few comprehensive independent variables Y_k (k = 1,2, ... ,m), as shown in Formula (3):

$$\begin{gathered} Y_k = a_{k1}X_1 + a_{k2}X_2 + \cdots + a_{ki}X_i + \cdots + a_{kn}X_n \\ Y = [Y_1 Y_2, ..., Y_m], X = [X_1 X_2, ..., X_n], m \leqslant n \\ Y_C = \sum_{k=1}^{m} Y_k v_k \end{gathered} \tag{3}$$

where n and m are the numbers of variables X and Y, and m is set according to demand; Y_C is the integrative factor; a_{ki} (k = 1,2, ... ,m, i = 1,2, ... ,n) are principal component coefficients; and v_k (k = 1,2, ... ,m) are component contribution rates, the calculations of which could refer to [15,16].

The integrative factor Y_C, which reflects the summarized information of original data and deletes unimportant factors, could replace original photovoltaic output in the following analysis.

Step 3. Grey correlation analysis (GCA):

In order to select similar days, the correlations between photovoltaic output and relative factors need to be analyzed first. The GCA, which has a good effect to solve the problem of multi-variables without obvious regularity, is a mature theory in this field and employed in this section [15,17].

The values of the integrative factors Y_C of the photovoltaic outputs form a basic sequence y, and the relative factors form compared sequences z_i (i = 1,2, ... ,p), the curve similarities of which reflect the degrees of relation.

$$\begin{gathered} y = \{y(k) \,|k = 1, 2, \cdots n\}, z_i = \{z_i(k) \,|k = 1, 2, \cdots n\} \\ \zeta_i(k) = \frac{\Delta_i(k)_{\min} + \rho\Delta_i(k)_{\max}}{\Delta_i(k) + \rho\Delta_i(k)_{\max}}, \Delta_i(k) = |y(k) - z_i(k)| \\ \gamma_i = \frac{1}{n}\sum_{k=1}^{n} \zeta_i(k), i = 1, 2, ..., p \end{gathered} \tag{4}$$

where $\Delta_i(k)_{\min}$ and $\Delta_i(k)_{\max}$ are the minimal and maximal values of $\Delta_i(k)$; $\rho \in (0, \infty)$ is the distinguish coefficient; n is the sequence length; p is the number of compared sequences; γ_i is the degree of correlation between y and z_i.

Step 4. Weighted similarity formula (WSF):

The WSF combined with all values of the degree of relation in Step 3 is adopted to calculate the degree of similarity $sim(k)$ between the day to predict and a given historical day [15].

$$\begin{gathered} sim(k) = 1/[\sum_{i=1}^{p} \theta_i \,|z_i(k) - z_i(0)| + \varepsilon], \theta_i = \gamma_i / \sum_{i=1}^{p} \gamma_i \\ k = 1, 2, ..., n, \varepsilon > 0 \end{gathered} \tag{5}$$

where p is the number of relative factors; n is the number of historical days; $z_i(k)$ is the normalized value of the i-th factor on day k; $z_i(0)$ is the normalized value of the i-th factor of the day to predict; θ_i is the weight of the relevant factor; γ_i is the degree of correlation above.

The sample data are sorted in descending order according to the similarity, and the front days would be selected as the similar days of the predicted day.

(2) Select similar days of F-H for load:

Step 1. Data preprocessing:

The factors that affect load mainly include the AQI value, temperature, humidity, weather type and day type. The factor data should be normalized or mapped to the range of [0,1] before calculation. The relation of day types, which include workdays and weekends, and their values are shown as follows: workday, 0.3; weekend, 0.8. In addition, emergency warning levels are added into the factors because the load would be greatly influenced by emergency warning policies: yellow alert, 0.3; orange alert, 0.6; red alert, 0.9; and none, 0.

Step 2–Step 4 are the same as above.

2.4. Prediction Model of the Wavelet Neural Network

There are various prediction models and algorithms suitable for photovoltaic output and load forecasts, such the artificial neural network (ANN) and its modified versions, the support vector machine, the extreme learning machine, *etc.* In this section, the WNN model that combines the ANN and the wavelets theory is selected to be the predictor because it is familiar to our team and it has the following advantages [18–22]:

(1) The ANN has characteristics such as self-learning, self-adaption and fault tolerance, and it is a universal function approximator.

(2) The motif and the whole structure of the WNN are set according to the theory of wavelet analysis, which could effectively extract the local information of the signal by multiresolution analysis and avoid the blindness of the structure design of the back propagation (BP) neural network.

(3) The WNN model has better learning ability and higher accuracy. In the same prediction tasks, the WNN with a simpler network structure possesses faster convergence speed.

The concepts of the ANN, the BP neural network and the wavelets theory are explained as follows to form the basic foundation framework of the WNN.

(1) Artificial neural network:

The ANN is a mathematical model that has the ability of parallel distributed information processing, based on the representation of neural activity in the human brain [18]. The most popular design for the ANN is the multi-layer feed forward network, which has an input layer, an output layer and one or more hidden layers. Each layer has a number of nodes or neurons, which consist of multiple inputs and a single output. A weight is associated with each input, while the input signal is multiplied by these weights. The neuron is responsible for the combination of these weighted inputs, and in accordance with an activation function, the output is determined.

(2) Back propagation neural network:

The BP neural network is a feed forward neural network, the signals of which are transmitted forward while the errors in reverse. Its basic learning rule is the steepest descent method, which minimizes the sum of squared errors according to the back-propagation to continuously adjust the weights and thresholds of the network [19].

(3) Wavelets theory:

The popularity of wavelets with compact supports is due mainly to their relation to the dyadic multiresolution analysis that dominates wavelet research [20]. Historically, the continuous wavelet transform came first, which is defined as below:

$$f_r(a,b) = \frac{1}{\sqrt{a}} \int_{-\infty}^{+\infty} x(t) \phi \left(\frac{t-b}{a} \right) dt, a > 0 \quad (6)$$

where $\phi(a, b)$ is a mother wavelet from which a family of wavelet daughters is obtained by scaling and translating it, thus by changing b (controlling the location) and a (determining the width of the wavelet and the frequency resolution).

(4) Wavelet neural network:

The WNN, based on the topology of the BP neural network, selects a certain wavelet basis function as the transfer function of nodes in the hidden layer, where the signal propagates forward while the error returns [21,22]. The basic structure of the WNN is shown in Figure 6.

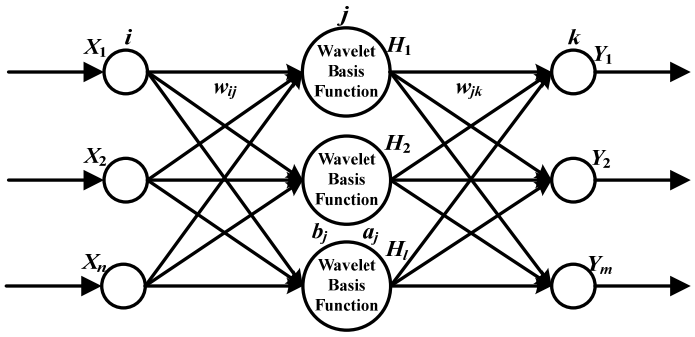

Figure 6. The basic structure of the wavelet neural network (WNN) prediction model.

Based on the strict theoretical background of wavelet analysis and the BP neural network, the WNN is able to adjust the weight and threshold values of the network and the scalability factors and

shift factors of the wavelet function, which gives the WNN more sensitive approximation capability and better fault-tolerant capability than the BP neural network.

As shown in Figure 6, X_1, X_2, ... , X_n are inputs of the WNN; H_1, H_2, ... , H_l are outputs of the nodes of the hidden layer; Y_1, Y_2, ... , Y_m, are outputs of the forecast; and n, l and m are the node numbers of the input layer, hidden layer and output layer.

If the input signals are x_i (i = 1,2, ... ,n), the output $h(j)$ of node j in the hidden layer is shown as follows:

$$h(j) = h_j\left(\frac{\sum_{i=1}^{n} w_{ij}x_i - b_j}{a_j}\right), j = 1, 2, ..., l \tag{7}$$

where w_{ij} is the connection weight between node i in the input layer and node j in the hidden layer; h_j is the wavelet basis function; and a_j and b_j are the scalability factor and shift factor of h_j.

Several wavelet basis functions have been proposed in the wavelets theory. Each basis function has its suitable application. In the WNN model of this paper, the Morlet wavelet, which is a non-orthogonal wavelet base without a scaling function, serves as the wavelet basis function because it is symmetrical and has a simple expression as below:

$$h_j(x) = \cos(\delta x)e^{-x^2/2} \tag{8}$$

where δ = 1.75, generally.

The output of node k in the output layer is shown as follows:

$$y(k) = \sum_{j=1}^{l} w_{jk}h(j), k = 1, 2, ..., m \tag{9}$$

where w_{jk} is the connection weight between node j in the hidden layer and node k in the output layer.

(5) Realization process of photovoltaic output (or load) forecast:

Step 1. Start.

Step 2. Import data on photovoltaic output (or load) and relative factors, which should be normalized or mapped to the range of [0,1].

Step 3. Select similar days of F-H for photovoltaic output (or load) forecast based on the PCA, the GCA and the WSF.

Step 4. Organize photovoltaic output (or load) data of similar days, three days before the day to predict and 3 h before the moment to predict to form the input and output data of the WNN.

Step 5. Initialize the parameters of the WNN, according to demand, such as node numbers (n, l and m), connection weights (w_{ij}, w_{jk}), wavelet parameters (a_j and b_j), error limit (e_0), iteration precision (Δy_0) and maximum number of iterations ($N_{\max}$).

Step 6. Repeatedly train the WNN through input and output data, according to Formulas (10) and (11). When the total forecast error $e < e_0$ or the iteration number $r > N_{\max}$, the training stops, and the network parameters that have a better fitting capacity for the original data are obtained.

$$e^r = \sum_{k=1}^{m} [y_0(k) - y^r(k)] \tag{10}$$

$$\begin{gathered} w_{ij}^{r+1} = w_{ij}^r + \eta_1 \frac{\partial e^r}{\partial w_{ij}^r}, w_{jk}^{r+1} = w_{jk}^r + \eta_2 \frac{\partial e^r}{\partial w_{jk}^r} \\ a_j^{r+1} = a_j^r + \eta_3 \frac{\partial e^r}{\partial a_j^r}, b_j^{r+1} = b_j^r + \eta_4 \frac{\partial e^r}{\partial a_j^r} \\ i = 1, 2, ..., n, j = 1, 2, ..., l, k = 1, 2, ..., m \end{gathered} \tag{11}$$

where $y_0(k)$ is the real values; η_1, η_2, η_3 and η_4 are the learning rates of w_{ij}, w_{jk}, a_j and b_j, which are set according to demand.

Step 7. Conduct the forecast for photovoltaic output (or load) using the WNN trained by Step 6 and analyze the results.

Step 8. The mean absolute percentage error (MAPE) and the mean squared error (MSE) are employed in this section to evaluate the forecast accuracy, which are shown as Formulas (12) and (13):

$$MAPE = \frac{100}{N}\sum_{i=1}^{N}\left|\frac{y_i - y'_i}{y_i}\right| \tag{12}$$

$$MSE = \frac{1}{N}\sum_{i=1}^{N}(y_i - y'_i)^2 \tag{13}$$

where N is the number of samples; y_i is the real value; y'_i is the forecast value.

The MAPE and the MSE will be small if the predicted values are very close to the true values and will be large if for some of the observations, the predicted and true values differ substantially.

Step 9. End.

3. The Dispatch of Power Systems Containing VPPs

3.1. The Construction of the VPP

The DERs that form the VPP could be the same or diverse, and their layout may be either concentrated or scattered. Information networks and high-level software architecture are employed inside the VPP to connect and control DERs. Therefore, there is no need to change the grid-connected structure and the distributed topology of DERs.

The construction of a VPP that consists of various DERs is shown in Figure 7.

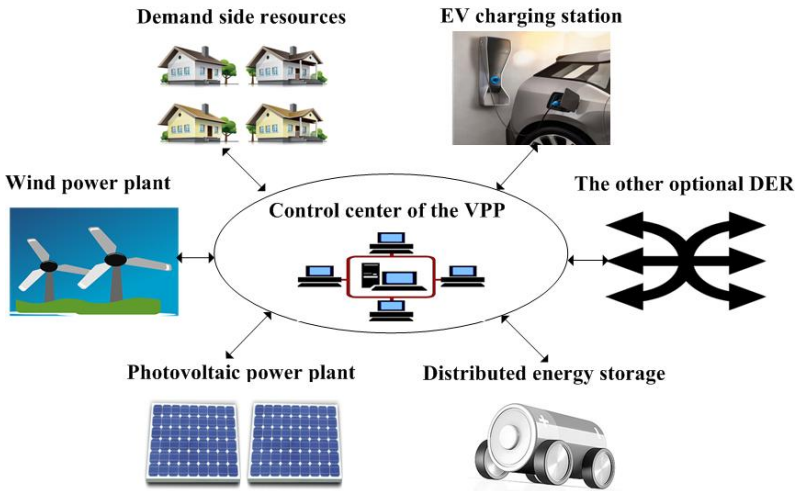

Figure 7. The construction of a virtual power plant (VPP). DER, distributed energy resource.

As shown in Figure 7, DERs that form the VPP in this paper could be wind power plants (WPP), photovoltaic power plants (PPP), demand side resources (DSR), electric vehicle charging stations (EVCS), distributed energy storage (DES), *etc.* The output of a VPP is the sum of all DER outputs, which can be predicted separately, inside the VPP. The characteristics of different DERs could be complementary, and the uncertainties could be offset to some degree, which gives the VPP better external characteristics, similar to conventional power plants, than scattered DERs.

3.2. The Dispatch Model Containing VPPs

The schematic diagram of VPPs participating in the dispatch is shown in Figure 8.

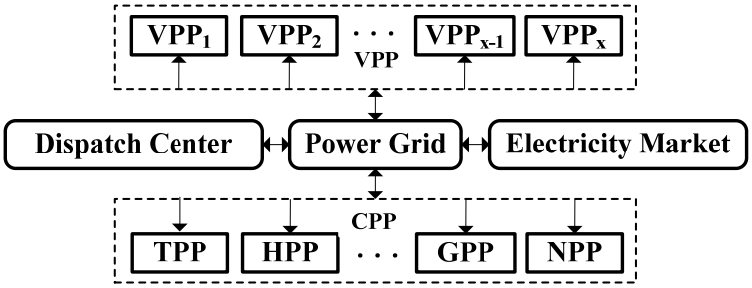

Figure 8. Schematic diagram of VPPs participating in the dispatch. TPP, thermal power plant; HPP, hydraulic power plant; GPP, geothermal power plant; NPP, nuclear power plant.

The VPP, as an autonomous entity, connects to the power grid just like other conventional power plants (CPP), such as thermal power plants (TPP), hydraulic power plants (HPP), geothermal power plants (GPP) and nuclear power plants (NPP). After the process of output prediction, the VPP uploads its output and other relevant information to the dispatch center and the electricity market through information and communication technology and receives instructions from the system.

Energy conservation and emissions reduction are the main objectives of the power system in the dispatch considering F-H weather. On the premise of satisfying the needs of the total load, the system preferentially takes in power generated by units with low emission and restricts (or even shuts down) units with high emission to some degree according to the operational constraints and economic characteristics of the units. In addition, several economic incentive measures are taken to encourage the development of new clean energy, such as wind power and photovoltaic power. Therefore, the VPP demonstrates its priority in dispatch via its advantage of low pollution and policies of fiscal subsidies. Generally, the higher the AQI level is, the more obvious the VPP's priority.

4. The Mathematical Model of Dispatch under F-H Weather

A multi-objective optimal dispatch model of a power system, containing several VPPs and conventional power plants (take the TPP as an example), is employed in this paper, comprehensively counting four objective functions (f_1–f_4) and six constraints (C_0–C_5) [23–27].

4.1. Objective Functions

(1) Minimizing generation cost and start-up (shut-down) cost of TPPs: f_1.

$$\begin{gathered} \min f_1 = \sum_{i=1}^{M} \sum_{t=1}^{T} [A_i(P_{Gi,t}) \cdot I_{Gi,t} + SU_{i,t} + SD_{i,t}] \\ A_i(P_{Gi,t}) = a_{Qi} \cdot (P_{Gi,t})^2 + b_{Qi} \cdot P_{Gi,t} + c_{Qi}, SU_{i,t} = C_{SUi} \cdot y_{Gi,t}, SD_{i,t} = C_{SDi} \cdot z_{Gi,t-1} \end{gathered} \tag{14}$$

where M is the number of thermal power units; T is the number of time intervals during the dispatch period; $P_{Gi,t}$ and $A_i(P_{Gi,t})$ are the output and generation cost of unit i in period t; $I_{Gi,t}$ is the running state of unit i in period t, with unit i on/off in period t when $I_{Gi,t} = 1/0$; a_{Qi}, b_{Qi} and c_{Qi} are the cost coefficients (constants) of unit i; $SU_{i,t}$ and $SD_{i,t}$ are the start-up and shut-down costs of unit i in period t; C_{SUi} and C_{SDi} are the cost coefficients of the start-up and shut-down of unit i; and $y_{Gi,t} = 1$ ($z_{Gi,t} = 1$) means that unit i is in the process of start-up (shut-down) in period t; otherwise, $y_{Gi,t} = 0$ ($z_{Gi,t} = 0$).

The relations among $y_{Gi,t}$, $z_{Gi,t}$ and $I_{Gi,t}$ (constraints C_0) are shown as Formula (15), which are additional equality constraints (C_{01}) and inequality constraints (C_{02}), because of the added variables ($y_{Gi,t}$ and $z_{Gi,t}$).

$$\begin{gathered} y_{Gi,t} - z_{Gi,t} = I_{Gi,t} - I_{Gi,t-1}, y_{Gi,t} - z_{Gi,t} \leqslant 1 \\ i = 1, 2, ...M, t = 1, 2, ...T \end{gathered} \tag{15}$$

where $I_{Gi,0}$ = 1/0 (t = 1) means that unit I is on/off before the dispatch period.

(2) Minimizing pollution emission of TPPs (considering the penalty factor of AQI): f_2.

Gaseous pollutants, such as SO_2, NO_x, PM10 and PM2.5, are the main emissions considered in this paper. The concept of nominal environmental compensation cost is introduced to transform the pollutant emission of the thermal power unit into emission cost.

$$\min f_2 = \sum_{i=1}^{M} [C_{Fi} \cdot \sum_{t=1}^{T} B_i(P_{Gi,t}) \cdot I_{Gi,t}], B_i(P_{Gi,t}) = a_{Wi} \cdot (P_{Gi,t})^2 + b_{Wi} \cdot P_{Gi,t} + c_{Wi} \tag{16}$$

where $B_i(P_{Gi,t})$ is the emission amount of unit i in period t; a_{Wi}, b_{Wi} and c_{Wi} are the pollutant discharge coefficients of unit i; and C_{Fi} is the cost coefficient of pollutant emissions of unit i.

In addition, the AQI level (L_{AQI}), as a penalty term, is added to the calculation of C_{Fi} to consider the effect of F-H in the dispatch. The economic punishment varies with L_{AQI} and the emission characteristic of the unit; namely, a unit with heavier pollution would receive more serious punishment when L_{AQI} is higher.

$$C_{Fi} = C_{Bi} \cdot \varphi(L_{AQI}), L_{AQI} = 1, 2, ..., 6 \tag{17}$$

where $\varphi(L_{AQI})$ is the growth factor function of emission cost and C_{Bi} is the cost coefficient of the pollutant emission of unit i when L_{AQI} = 1 (the air condition is excellent); namely, $\varphi(1)$ = 1 and $C_{Fi} = C_{Bi}$. Generally, the worse the emission characteristics of a unit is, the larger the C_{Bi} value, which causes the unit to stay in an inferior position in the dispatch considering the environmental benefits.

Therefore, it could be deduced according to the above analysis that $\varphi(L_{AQI})$ might be an increasing function, which would be supposed to be a linear one since there are no studies on this expression.

$$\varphi(L_{AQI}) = 1 + \alpha \cdot (L_{AQI} - 1), L_{AQI} = 1, 2, ..., 6 \tag{18}$$

where α is the empirical value of the proportionality coefficient of $\varphi(L_{AQI})$, obtained from the comprehensive analysis of the policies, F-H condition and emission characteristic of the units.

(3) Minimizing carbon emission of TPPs: f_3.

Carbon emission is namely greenhouse gas emission, which mainly includes CO_2, N_2O, CH_4 and O_3. Only CO_2 is discussed in this paper, because the other greenhouse gases could be converted into CO_2 equivalent.

$$\min f_3 = \sum_{i=1}^{M} (C_{Xi} \cdot c_{ei} \cdot e_{Gi} \cdot \sum_{t=1}^{T} P_{Gi,t}) \tag{19}$$

where C_{Xi}, c_{ei} and e_{Gi} are the cost coefficient of carbon emission, the coal consumption rate and the carbon discharge coefficient of unit i.

(4) Minimizing generation cost of VPPs: f_4.

It is assumed that the generation cost of a DER and that of its output have a linear relationship to simplify the dispatch model, based on a comprehensive consideration of the basic construction cost,

operation and maintenance costs and control cost of DERs. Similarly, the generation cost and output of a VPP have a linear relationship.

$$\min f_4 = \sum_{k=1}^{n} (w_k \cdot \sum_{t=1}^{T} P_{VPPk,t}), w_k = \sum_{j=1}^{m_k} \delta_{k,j} \cdot w_{k,j} \tag{20}$$

where n is the number of VPPs; w_k is the generation cost coefficient of VPP_k; $P_{\mathrm{VPP}k,t}$ is the output of VPP_k in period t; m_k is the number of DERs inside VPP_k; $\delta_{k,j}$ is the capacity proportion of DER_j inside VPP_k; and $w_{k,j}$ (constant) is the generation cost coefficient of DER_j inside VPP_k. Therefore, w_k would be a constant if the types of DERs and $\delta_{k,j}$ are known.

4.2. Constraints

(1) System power balance constraints: C_1.

$$\sum_{i=1}^{M} P_{Gi,t} + \sum_{k=1}^{n} P_{VPPk,t} = P_{Dt}, t = 1, 2, ..., T \tag{21}$$

where P_{Dt} is the total load in period t.

(2) Output limits of TPPs and VPPs: C_2.

$$\begin{gathered} P_{\min-Gi} \cdot I_{Gi,t} \leqslant P_{Gi,t} \leqslant P_{\max-Gi} \cdot I_{Gi,t}, P_{\min-VPPk} \leqslant P_{VPPk,t} \leqslant P_{\max-VPPk} \\ i = 1, 2, ..., M, t = 1, 2, ..., T, k = 1, 2, ..., n \end{gathered} \tag{22}$$

where P_{min-Gi} and $P_{\mathrm{m}ax-Gi}$ are the minimum and maximum outputs of thermal power unit I; the counterparts of VPP_k are $P_{min-VPPk}$ and $P_{\mathrm{m}ax-VPPk}$.

(3) System reserve constraints: C_3.

$$\sum_{i=1}^{M} P_{\max-Gi} \cdot I_{Gi,t} + \sum_{k=1}^{n} P_{\max-VPPk} \geqslant P_{Dt} + S_{Dt}, t = 1, 2, ..., T \tag{23}$$

where S_{Dt} is the total system reserve in period t.

(4) Ramping constraints of TPPs: C_4.

$$\left| P_{Gi,t} - P_{Gi,t-1} \right| \leqslant Q_i, i = 1, 2, ..., M, t = 2, 3, ..., T \tag{24}$$

where Q_i is the limit value of output change of unit i.

(5) The maximal start/stop count limits: C_5.

The VPP is in the running state all of the time, except during maintenance in the dispatch period, so the start/stop constraints consider only TPPs. These constraints are expressed as minimal on/off time limits in published research works, which are transformed into maximal start/stop counts to simplify the complexity of calculation in this paper.

$$\sum_{t=2}^{T} \left| I_{Gi,t} - I_{Gi,t-1} \right| \leqslant J_{\max-i}, i = 1, 2, ...M \tag{25}$$

where $J_{\max-i}$ is the maximum start/stop count of unit i.

5. Solving the Optimal Dispatch Model Based on MILP

Mixed integer linear programming (MILP) [24] and the MATLAB toolbox Yalmip are employed to solve the above multi-objective optimal dispatch model. The MILP, which has no iteration process, is good at handling power system optimal dispatch problems because of its nice astringency, good optimality and simple expression of constraints. Yalmip is a free toolbox developed by Lofberg, and the greatest advantage lies in its simple and general modeling language.

5.1. Model Simplification

The objectives in this paper are all about costs that could be added up to form a total cost; the linear weighted sum method [28] is adopted to simplify the calculation in the early study.

$$\begin{gathered} F = \min_{X} \sum_{r=1}^{4} \beta_r \cdot f_r(X), X = [P_{Gi,t}, I_{Gi,t}, P_{VPPk,t}] \\ s.t. \begin{cases} H_p(X) = 0, (p = 1, 2, ..., MT + T) \Leftrightarrow C_{01}, C_1 \\ G_q(X) \leqslant 0, (q = 1, 2, ..., Q) \Leftrightarrow C_{02}, C_2, C_3, C_4, C_5 \\ Q = MT + 2(M + n)T + T + 2M(T - 1) + M \end{cases} \end{gathered} \tag{26}$$

where X and F are the decision variable set and the comprehensive objective function; β_r is the weight of f_r; C_0–C_5 are constraints; H_p (p = 1,2, … ,MT+T) are equality constraints; G_q (q = 1,2, … ,Q) are inequality constraints; and Q is the number of inequality constraints.

Usually, the selections of the weights depend on the choices of the decision maker or field practical experience. Besides, Formula (27) is adopted to calculate weights, as well.

$$\beta_r = \frac{\dfrac{1}{f_r(X^*)}}{\sum\limits_{r=1}^{4} \dfrac{1}{f_r(X^*)}} \tag{27}$$

where $f_r(X^*)$ is the optimal value of the single objective problem of $f_r(X)$.

5.2. Linearization of Objective Functions

The objectives, such as generation cost and emission of thermal power units, could be linearized based on the piecewise linearization, which has better performance on the functions with low nonlinearity degree, to fit the solver Yalmip and simplify the calculation [25]. The linearization formulas are shown as follows:

$$\begin{gathered} f(x) = ax^2 + bx + c \\ f = f(x_{\min}) + \sum_{u=1}^{U} k_u x_u, x = x_{\min} + \sum_{u=1}^{U} x_u \\ 0 \leqslant x_u \leqslant \Delta X_u, u = 1, 2, ..., U \\ \Delta X_u = X_u - X_{u-1}, X_0 = x_{\min}, X_U = x_{\max} \end{gathered} \tag{28}$$

where $x_{\min}$ and $x_{\max}$ are the minimum and maximum values of variable x; X_u is the value of the segment point of segment u; U is the number of segments; and k_u is the slope of segment u.

If x is in segment u ($X_{u-1} \leqslant x \leqslant X_u$):

$$\begin{gathered} x_{u1} = 0, u1 = u + 1, u + 2, ..., U \\ x_{u2} = \Delta X_{u2}, u2 = u - 1, u - 2, ..., 1 \end{gathered} \tag{29}$$

5.3. Model Solving

The Yalmip toolbox is employed on the MATLAB 2014a platform to solve a power system optimal dispatch model containing VPPs under F-H weather, according to the steps as follows:

Step 1. Start;

Step 2. Import data of load, AQI level (L_{AQI}), outputs and relative information of thermal power units and VPPs, basic parameters of DERs inside VPPs and other useful information;

Step 3. Define column vector X of unknown variables and calculate row vector V of coefficients of the comprehensive objective function according to Formula (26): $F = V \times X$;

Step 4. Set all constraints W according to Formula (26): $W = W + \text{set}(C_i)$, $i = 1,2,...,5$;

Step 5. Set the empirical value of proportionality coefficient α of $\varphi(L_{AQI})$ according to Formula (18);

Step 6. Solve the model by the Yalmip toolbox in MATLAB: result = solvesdp(W, F);

Step 7. Export results and analyze;

Step 8. End.

6. Case Study

6.1. Photovoltaic Output and Load Forecasts under F-H

According to the methods mentioned in Section 2, the data of the AQI value, temperature (minimum and maximum), weather type, day type, photovoltaic output and load of a certain region in Baoding, China, during the period from 1 December 2013–26 March 2014 were gathered to conduct photovoltaic output and load forecasts. To verify the analysis of the influence of F-H, the prediction results of 27 March 2014 (AQI = 305, overcast) are shown as follows (both considering and ignoring F-H).

As shown in Figure 9, the red curve (with AQI) is closer to the black curve (real value) than the blue curve (without AQI); in Table 2, the MAPE and the MSE with AQI are much smaller than those without AQI, which indicates that the prediction accuracy of the photovoltaic output is higher if F-H is considered.

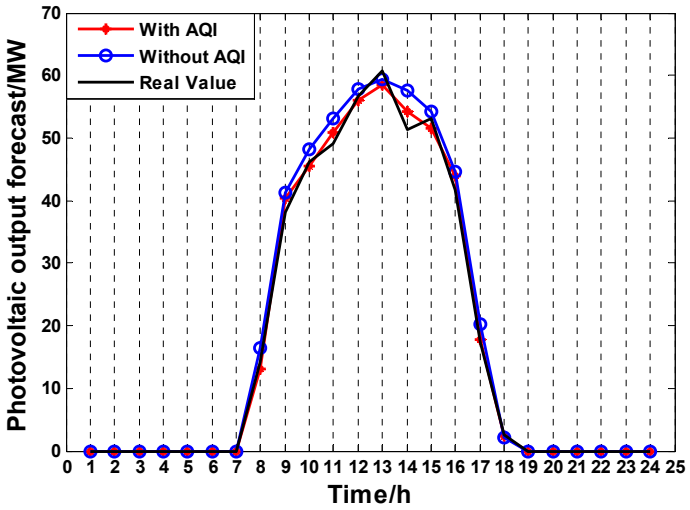

Figure 9. Result comparison of the photovoltaic output forecast with and without AQI.

Table 2. MAPE and MSE of the photovoltaic output forecast.

Case	MAPE (%)	MSE
With AQI	4.4181	2.9696
Without AQI	8.4941	8.5712

As shown in Figure 10, the blue curve (without AQI) is higher on average than the black curve (real value), especially in the period of peak load, while the red curve (with AQI) is closer to the black curve; in Table 3, the MAPE and the MSE with the AQI are also smaller than those without AQI, which indicates that the prediction accuracy of the load is higher if F-H is considered.

In other words, the prediction accuracy is higher because photovoltaic outputs and loads of similar days are much closer to those of the day being predicted when the AQI factor is included. During the similar days of F-H, the atmosphere factors, the operating states of PV panels, the electric power consumption of the whole society and the macroscopic readjustment of the Chinese government are similar, as well. The WNN model with better learning ability is able to catch the change pattern of photovoltaic outputs and loads to form more accurate predictions.

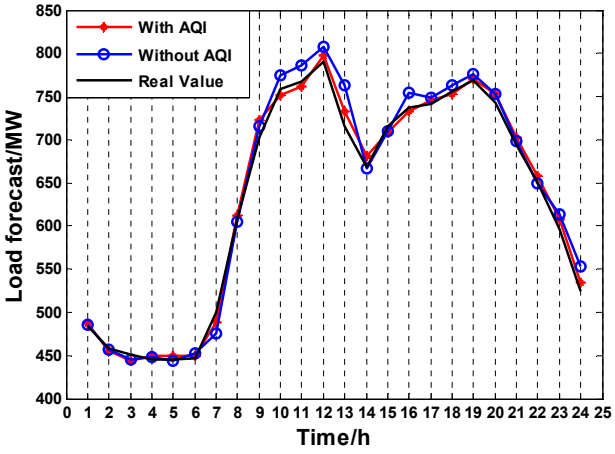

Figure 10. Result comparison of the load forecast with and without AQI.

Table 3. MAPE and MSE of the load forecast.

Case	MAPE (%)	MSE
With AQI	2.6662	167.0492
Without AQI	3.7528	523.0842

6.2. The Dispatch under F-H Weather

(1) Case description:

There are two thermal power units (G_1 and G_2) and two VPPs (VPP_1 and VPP_2) supplying the total load, the forecast curve of which is shown in Figure 10, of a certain region in Baoding, China, on 27 March 2014 (AQI = 305, L_{AQI} = 6). Some relative parameters of G_1 and G_2 are listed in Tables 4 and 5.

Table 4. The cost and emission coefficients of G_1 and G_2.

Unit	a_{Qi} yuan/MW^2	b_{Qi} yuan/MW	c_{Qi} yuan	a_{Wi} kg/MW^2	b_{Wi} kg/MW	c_{Wi} kg
G_1	0.018	38.306	1243.531	3.380	−3.550	5.426
G_2	0.011	36.328	1658.570	6.490	−5.554	5.090

Table 5. The other information of G_1 and G_2.

Unit	P_{min-Gi} MW	P_{max-Gi} MW	e_{Gi} t/MW	c_{ei} t/t	C_{Bi} yuan/t	C_{Xi} yuan/t	C_{SUi} yuan	C_{SDi} yuan	J_{max-i}
G_1	35	210	0.350	1.6	21	13	330	110	5
G_2	130	325	0.340	1.8	16	14	430	140	4

VPP_1 consists of a wind power plant (WPP_1, 100 MW), a photovoltaic power plant (PPP_1, 80 MW) and an efficiency power plant (EPP, 90 MW); VPP_2 consists of a WPP (WPP_2, 80 MW), a PPP (PPP_2, 60 MW) and an electric vehicle charging station (EVCS, 70 MW).

An EPP implements all kinds of electricity-saving strategies in a certain region, and the electricity saved becomes its virtual output, which is equivalent to building a new power plant or enlarging the capacity of an old one. The control strategies and implementation of an EPP rely on advanced communication and information technology [29]. An EVCS aggregates a large number of EVs, the charge-discharge patterns of which are rationally controlled to realize load shifting. Thus, the charge-discharge control strategies of EVs are the fundamental tasks of an EVCS [30].

The main focus of this case is the plan of green economic dispatch between the power system and VPPs under F-H weather. The characteristics of DERs inside VPPs will be researched in a future study. Therefore, it is hypothesized that the EPP and EVCS act only as special generation units, and their outputs could be controlled and adjusted according to demand within capacities, which could simplify the dispatch model.

The output forecast curves of VPP_1 and VPP_2, which are shown in Figure 11, would be available by adding the forecast curves of the WPP and PPP and the capacity of the EPP (90 MW, VPP_1) or the EVCS (70 MW, VPP_2).

The cost coefficients (yuan/MW) of the WPP, the PPP, the EPP and the EVCS are 414, 1170, 278 and 670, respectively [29–31]. In addition, financial subsidies have been used to encourage the development of DERs without pollution. To simplify the calculation, it is hypothesized that the basic rate of subsidization of all DERs is 40%.

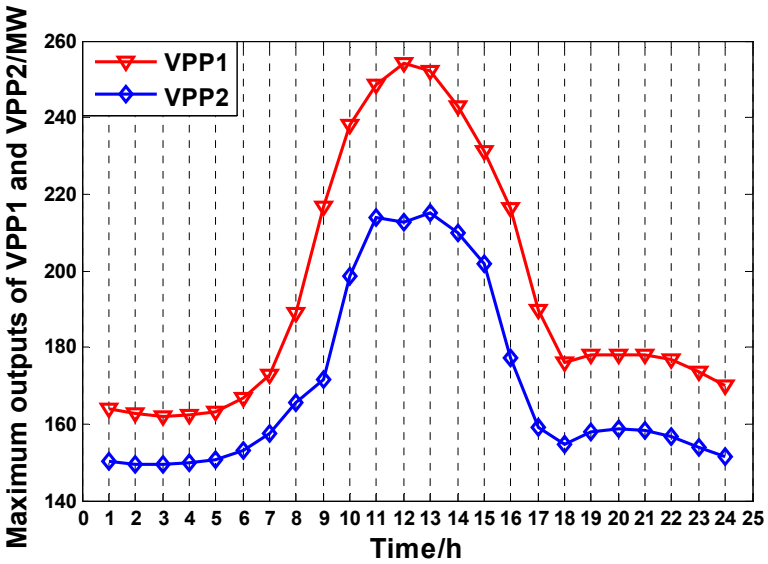

Figure 11. Maximum output forecasts of VPP_1 and VPP_2.

(2) Result analysis:

The dispatch results are shown in Figure 12 (L_{AQI} = 6; the proportionality coefficient of the growth factor function of emission cost α = 1.5; weights of the objective functions without AQI: β_1 = 0.1089, β_2 = 0.2030, β_3 = 0.6275 and β_4 = 0.0606; with AQI: β_1 = 0.1286, β_2 = 0.0489, β_3 = 0.8017, β_4 = 0.0208).

It is shown in Figure 12 that 70.35% of daily load is supplied by thermal power units (G_1 and G_2) with a cost advantage, and the other 29.65% is left for VPPs (VPP_1 and VPP_2) when F-H is ignored. The reasons could be described as follows. First, G_1 and G_2 receive less economic punishment according to Formula (18) and have a higher dispatch priority with their cost advantage when the effect of F-H is ignored. Second, the cost coefficients of DERs inside VPP_1 and VPP_2 are much larger. Thus, only VPP_1

with a lower cost shares more load requirements, and the output of VPP_2 is rarely adopted, which results in the waste of clean DERs.

Conversely, if F-H is considered, 54.98% of the daily load is supplied by VPPs that contain many clean DERs, which is much larger than the former condition (>29.65%), and only 45.02% (<70.35%) is left for the thermal power units. G_1 and G_2 incur a much higher emission cost, because the AQI factor is considered, which greatly weakens the generation cost advantages of thermal power units. Therefore, VPP_1 and VPP_2 gain a higher dispatch priority, because DERs have less or even no pollution, which makes full use of clean energy. Although G_1 and G_2 could at least run with minimal output at a much higher expense to satisfy the load requirement, they would be shut down if VPPs have larger capacities or there are other units with lower pollution and cost.

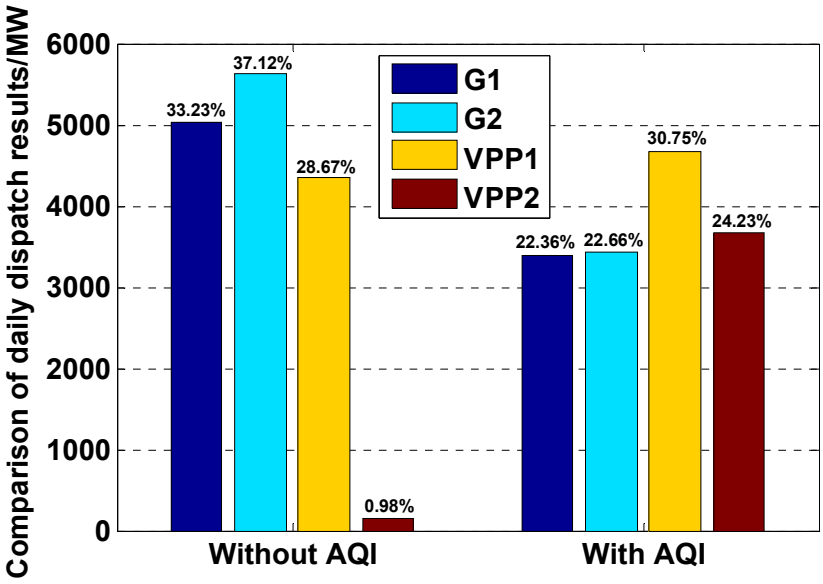

Figure 12. Comparison of daily dispatch results without and with AQI.

The curves of variations of cost and emission under different AQI levels are shown in Figure 13 (the proportionality coefficient of the growth factor function of emission cost α = 1.5).

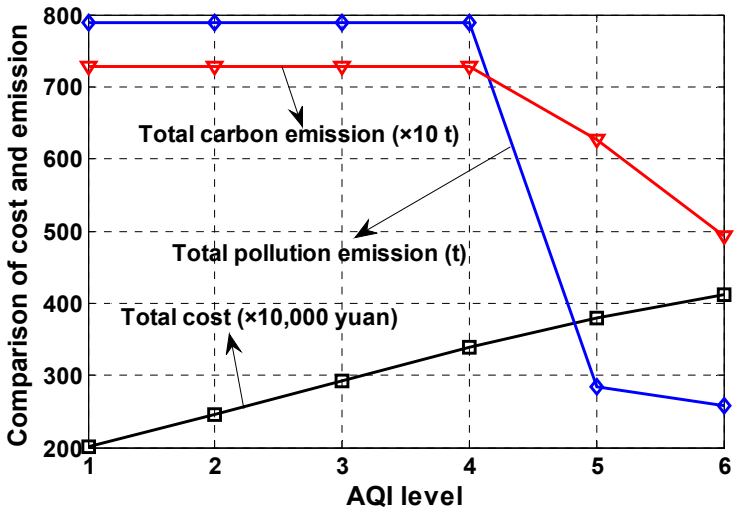

Figure 13. Variations of cost and emission under different AQI levels.

It can be seen in Figure 13 that the total cost increases with increasing AQI level (1–6) because the emission cost increases significantly according to Formulas (17) and (18). When the AQI level is smaller than four, G_1 and G_2 could still afford the rising emission cost. Therefore, the outputs of the units remain unchanged, and the total carbon emission and total pollution emission remain at the same level. However, when the AQI level increases from 4–6, the total carbon emission and pollution emission decrease significantly because G_1 and G_2 cannot endure a heavy emission punishment and must reduce their outputs to control emission, which allows the clean DERs inside VPPs to be fully used.

The above situations are consistent with the emergency warning policies of the Chinese government. When the air condition is worse than moderate pollution ($L_{AQI} > 4$), the Chinese government forcibly restricts the outputs of conventional thermal power units (or even shuts them down). Therefore, the method that modifies the emission cost by adding the AQI factor has a certain practical significance and research value.

The curves of variations of cost and emission under different values of α (the proportionality coefficient of the growth factor function of emission cost) are shown in Figure 14 ($L_{AQI} = 6$).

α is an empirical value that could be drawn from the comprehensive analysis of policies, F-H condition and emission characteristics of the units. It can be seen in Figure 14 that the total cost increases with increasing α according to Formulas (17) and (18). However, the total carbon emission and total pollution emission are not always decreasing. Therefore, an optimal value of α must be selected to both control the total cost and reduce emissions of carbon and pollutants. The optimal value of α is 1.5 ($L_{AQI} = 6$) in Figure 14, which is adopted in this paper.

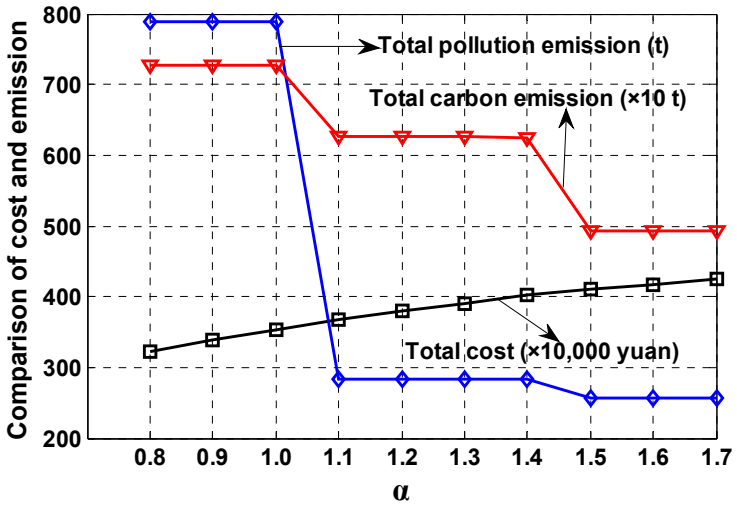

Figure 14. Variations of cost and emission under different values of α.

7. Conclusions

With the growing harmful effects of F-H around China, this paper has employed the WNN prediction model to forecast photovoltaic output and power load based on the analysis of the influence of F-H. On that basis, the concept of the VPP is adopted to handle the dispatch problem of multiple DERs connecting to the power grid, and a multi-objective optimal dispatch model of a power system containing VPPs, with the goals of energy conservation and emission reduction under F-H weather, is constructed based on traditional unit commitment. Several conclusions have been drawn from the above study:

(1) The influence of F-H on the photovoltaic output and load forecasts cannot be ignored, and the prediction accuracy could be improved effectively by selecting similar days of F-H to account for the influence of F-H.

(2) F-H has a great influence on the power system dispatch with the goals of energy conservation and emission reduction. If the AQI factor is considered, VPPs would generate more electricity, and thermal power units would be restricted, based on the comprehensive consideration of the overall benefit of the power system and macro policies, such as emission punishment, financial subsidies and emergency warning measures. Therefore, clean DERs would be fully used, and air pollution would be controlled to some degree.

(3) The influence of F-H on the output characteristics and control strategies of DERs inside VPPs has not been discussed in this paper; this will be studied in later papers.

Acknowledgments: The authors would like to acknowledge the financial support from the National High Technology Research and Development Program of China (No. 2015AA050104) and the Fundamental Research Funds for the Central Universities.

Author Contributions: Yajing Gao proposed the original idea and analyzed and double-checked the results and the whole manuscript. Huaxin Cheng carried out the main research tasks and wrote and translated the full manuscript. Jing Zhu helped to collect data and to translate the original manuscript. Haifeng Liang and Peng Li contributed to the interpretation of the results.

Conflicts of Interest: The authors declare no conflict of interest.

References

1. Zhang, X.D.; Liang, J. From London to Beijing: A comparison and reflexion on smog controls in China and Britain. *Frontiers* **2014**, *2*, 52–63.
2. Cheng, W.L.; Kuo, Y.C.; Lin, P.L.; Chang, K.-H.; Chen, Y.-S.; Lin, T.-M.; Huang, R. Revised air quality index derived from an entropy function. *Atmos. Environ.* **2004**, *38*, 383–391. [CrossRef]
3. Walling, R.A.; Saint, R.; Dugan, R.C.; Burke, J.; Kojovic, L.A. Summary of distributed resources impact on power delivery systems. *IEEE Trans. Power Deliv.* **2008**, *23*, 1636–1644. [CrossRef]
4. Chaouachi, A.; Kamel, R.M.; Andoulsi, R.; Nagasaka, K. Multi objective intelligent energy management for a microgrid. *IEEE Trans. Ind. Electron.* **2013**, *60*, 1688–1699. [CrossRef]
5. Chen, L.J.; Mei, S.W. An integrated control and protection system for photovoltaic microgrids. *CSEE J. Power Energy Syst.* **2015**, *1*, 36–42. [CrossRef]
6. Mashhour, E.; Moghaddas, T.S. Bidding strategy of virtual power plant for participating in energy and spinning reserve markets-Part I: Problem formulation. *IEEE Trans. Power Syst.* **2011**, *26*, 949–956. [CrossRef]
7. Giuntoli, M.; Poli, D. Optimized thermal and electrical scheduling of a large scale virtual power plant in the presence of energy storages. *IEEE Trans. Smart Grid* **2013**, *22*, 765–771. [CrossRef]
8. Lu, Z.X.; Ye, X.; Qiao, Y.; Min, Y. Initial exploration of wind farm cluster hierarchical coordinated dispatch based on virtual power generator concept. *CSEE J. Power Energy Syst.* **2015**, *1*, 62–67. [CrossRef]
9. Arslan, O.; Karasan, O.E. Cost and emission impacts of virtual power plant formation in plug-in hybrid electric vehicle penetrated networks. *Energy* **2013**, *60*, 116–124. [CrossRef]
10. Vasirani, M.; Kota, R.; Cavalcante, R.L.G.; Ossowski, S.; Jennings, N.R. An agent-based approach to virtual power plants of wind power generators and electric vehicles. *IEEE Trans. Smart Grid* **2013**, *4*, 1314–1322. [CrossRef]
11. Wille, H.B.; Erge, T.; Wittwer, C. Decentralized optimization of a cogeneration in virtual power plants. *Sol. Energy* **2010**, *84*, 604–601. [CrossRef]
12. Wan, C.; Zhao, J.; Song, Y.H.; Xu, Z.; Lin, J.; Hu, Z.C. Photovoltaic and Solar Power Forecasting for Smart Grid Energy Management. *CSEE J. Power Energy Syst.* **2015**, *1*, 38–46. [CrossRef]
13. Kang, C.Q.; Zhou, A.S.; Wang, P.; Zheng, G.; Liu, Y. Impact analysis of hourly weather factors in short-term load forecasting and its processing strategy. *Power Syst. Technol.* **2006**, *30*, 5–10.
14. Nobre, A.M.; Karthik, S.; Liu, H.; Yang, D.; Martins, F.R.; Pereira, E.B.; Rüther, R.; Reindl, T.; Peters, I.M. On the impact of haze on the yield of photovoltaic systems in Singapore. *Renew. Energy* **2016**, *89*, 389–400. [CrossRef]
15. Li, J.; Gao, Y.J.; Liu, J.P.; Ji, W.; Wang, N. The research of grid short-term load forecasting considering with air quality index. In Proceedings of the 2014 International Conference on Power System Technology (POWERCON 2014), Chengdu, China, 22–24 October 2014; pp. 852–857.

16. Stock, J.H.; Watson, M.W. Forecasting using principal components from a large number of predictors. *J. Am. Stat. Assoc.* **2002**, *97*, 1167–1179. [CrossRef]
17. Jin, M.; Zhou, X.; Zhang, Z.M.; Tentzeris, M.M. Short-term power load forecasting using grey correlation contest modeling. *Expert Syst. Appl.* **2012**, *39*, 773–779. [CrossRef]
18. Beccali, M.; Cellura, M.; Brano, V.L.; Marvuglia, A. Forecasting daily urban electric load profiles using artificial neural networks. *Energy Convers. Manag.* **2004**, *45*, 2879–2900. [CrossRef]
19. Hippert, H.S.; Pedreira, C.E.; Souza, R.C. Neural networks for short-term load forecasting: A review and evaluation. *IEEE Trans. Power Syst.* **2001**, *16*, 44–55. [CrossRef]
20. Mandal, P.; Madhira, S.T.S.; Meng, J.; Pineda, R.L. Forecasting power output of solar photovoltaic system using wavelet transform and artificial intelligence techniques. *Procedia Comput. Sci.* **2012**, *12*, 332–337. [CrossRef]
21. Chen, Y.; Luh, P.B.; Guan, C.; Zhao, Y.; Michel, L.D.; Coolbeth, M.A.; Friedland, P.B.; Rourke, S.J. Short-term load forecasting: Similar day-based wavelet neural networks. *IEEE Trans. Power Syst.* **2010**, *25*, 322–330. [CrossRef]
22. Gao, Y.J.; Liu, D.; Cheng, H.X.; Tian, L.; Peng, L. State Key Laboratory of Alternate Electrical Power System With Renewable Energy Sources. Predictor-Corrector Model of Wind Power Forecast Based on Data-driven. *Proc. CSEE* **2015**, *35*, 2645–2653.
23. Cheng, H.X.; Gao, Y.J.; Zhang, J.; Li, R.; Liang, H. The power system multi-objective optimization dispatching containing virtual power plant. In Proceedings of the 2014 International Conference on Power System Technology (POWERCON 2014), Chengdu, China, 22–24 October 2014; pp. 3316–3321.
24. Viana, A.; Pedroso, J.P. A new MILP-based approach for unit commitment in power production planning. *Int. J. Electr. Power Energy Syst.* **2013**, *44*, 997–1005. [CrossRef]
25. Carrión, M.; Arroyo, J.M. A computationally efficient mixed-integer linear formulation for the thermal unit commitment problem. *IEEE Trans. Power Syst.* **2006**, *21*, 1371–1378. [CrossRef]
26. Xing, H.J.; Cheng, H.Z.; Zhang, L.B. Demand Response Based and Wind Farm Integrated Economic Dispatch. *CSEE J. Power Energy Syst.* **2015**, *1*, 47–51. [CrossRef]
27. Gao, Y.J.; Liu, J.P.; Yang, J.; Liang, H.; Zhang, J. Multi-Objective Planning of Multi-Type Distributed Generation Considering Timing Characteristics and Environmental Benefits. *Energies* **2014**, *7*, 6242–6257. [CrossRef]
28. Marler, R.T.; Arora, J.S. The weighted sum method for multi-objective optimization: New insights. *Struct. Multidiscip. Optim.* **2010**, *41*, 853–862. [CrossRef]
29. Li, H.Z.; Wang, B.; Guo, S. Analytic Model and Benefits Measurement of Efficiency Power Plant Participating in Market Bidding Transaction in Smart Grid Environment. *Power Syst. Technol.* **2012**, *36*, 111–116.
30. Liu, Z.P.; Wen, F.S.; Ledwich, G. Optimal planning of electric-vehicle charging stations in distribution systems. *IEEE Trans. Power Deliv.* **2013**, *28*, 102–110. [CrossRef]
31. Yin, X.; Chen, W.Y. Cost of Carbon capture and storage and renewable energy generation based on the learning curve method. *J. Tsinghua Univ. (Sci. Technol.)* **2012**, *52*, 243–248.